Particle-size dependence of phase stability and amorphouslike phase formation in nanometer-sized Au-Sn alloy particles

H. Yasuda,[1,*] K. Mitsuishi,[2] and H. Mori[3]
[1]*Department of Mechanical Engineering, Faculty of Engineering, Kobe University, Rokkodai, Nada, Kobe 657-8501, Japan*
[2]*National Research Institute for Metals, Sakura, Tsukuba, Ibaraki 305-0003, Japan*
[3]*Research Center for Ultra-High Voltage Electron Microscopy, Osaka University, Yamadaoka, Suita, Osaka 565-0871, Japan*
(Received 28 July 2000; revised manuscript received 21 February 2001; published 30 July 2001)

The effect of particle size on the phase stability in nanometer-sized Au-Sn alloy particles has been studied by transmission electron microscopy. When the composition of alloy particles falls in the two-phase region in the phase diagram for the bulk material, two phases expected from the phase diagram were produced in particles of larger than 10 mm in diameter, whereas no interfaces between two different phases can be recognized in the interior of individual alloy particles to produce an amorphouslike phase below 6-nm-sized alloy particles. The amorphouslike phase directly changes into a liquid phase with increasing temperature and then the reversible transformation occurs with decreasing temperature. The changes in the free energy in nm-sized particles bringing about melting temperature depression may play an important role in the stability of amorphouslike phases.

DOI: 10.1103/PhysRevB.64.094101 PACS number(s): 64.70.−p

I. INTRODUCTION

Small particles in the size range from a few to several nanometers (nm) often exhibit structures and phase stabilities which are significantly different from those of the corresponding bulk materials. As a typical example, such phase transition temperatures as melting point and order-disorder critical temperature are remarkably reduced with decreasing size of particles.[1–5] However, to the authors' knowledge, studies on the phase stability and transformation in nm-sized binary alloy particles are few.[6,7]

In the present work, we studied the Au-Sn binary system by transmission electron microscopy (TEM), in order to see the phase stability of alloy particles as a function of particle size. In the phase diagram of the bulk Au-Sn system, two intermediate phases (i.e., Au_5Sn and AuSn) are formed in the range from 0 to 60 at. % Sn and the two-phase region consisting of Au_5Sn and AuSn exists.[8] The structures and chemical compositions of nm-sized Au-Sn alloy particles in this two-phase region have been investigated *in situ* by TEM. Furthermore, the thermal stability of the alloy particles has been investigated by *in situ* annealing experiments.

II. EXPERIMENTAL PROCEDURES

Preparation of size-controlled Au$\sim$35 at. % Sn alloy particles was carried out using a double-source evaporator installed in the specimen chamber of a TEM. The evaporator consists of two spiral-shaped tungsten filaments. An amorphous carbon film mounted on a molybdenum grid or a cleaved graphite substrate were used as a supporting film. They were baked out at about 1073 K for 60 s prior to the experiments. Using this evaporator, gold was first evaporated from one filament to produce nm-sized gold particles on the supporting film. Tin was then evaporated from the other filament onto the same film. In cases where gold particles produced on the film were less than approximately 10 nm in diameter, vapor-deposited tin atoms quickly dissolved into gold particles and alloy particles were formed.[9] By contrast, when gold particles were larger than this size, dissolution of tin was incomplete and only inhomogeneously alloyed particles were formed. Both types of particles were then annealed in the microscope at about 500 K for 300 s and slowly cooled from the annealing temperature to room temperature in 900 s. This annealing treatment was done in an attempt to allow high atomic mobility in the particles which would bring about the equilibrium degree. According to the bulk diffusion constant,[10] the annealing period employed (i.e., 300 s) is long enough for constituent atoms to migrate over a distance of about 10 nm, which is larger than half a maximum diameter of particles used in the present work.

The structure and chemical composition of the annealed alloy particles were then studied by TEM at room temperature as a function of the particle size. The chemical composition of individual particles on the film was analyzed by energy-dispersive x-ray spectroscopy (EDS). The analyses were carried out using an electron probe of approximately 1 nm in diameter. The characteristic x ray of gold and tin were collected with an ultrathin window x-ray detector at a high take-off angle of 68°. The background was simulated by curve fitting, and then subtracted. The chemical composition of particles was calculated from an intensity ratio of Sn $L\,\alpha_1$ to Au $L\,\alpha_1$ peak, using sensitivity factors. In the present experiments, total x-ray counts under either the Au $L\,\alpha_1$ or Sn $L\,\alpha_1$ peaks are from several hundreds to a thousand and are low, because only approximately 200–300 atoms are contained in the analyzed region. It was confirmed from the preliminary experiments that the compositional error depending on total x-ray counts is within ± 2 at. % Sn. On the other hand, the error of compositions determined by measurements repeated at three close positions in the individual clusters was less than ± 1 at. % Sn. Consequently, it is expected that the total error of compositions was within ± 3 at. % Sn. The error in composition of particles produced on the film was controlled to be less than ± 3 at. % Sn.

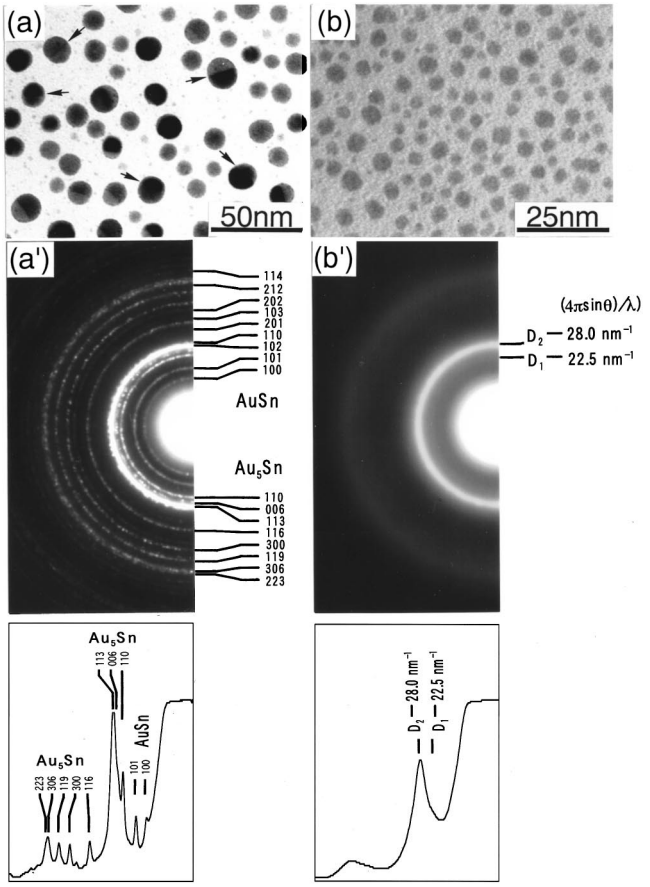

FIG. 1. Typical examples of size-controlled Au ~35 at. % Sn particles. (a) A BFI of particles of 7–20 nm in mean diameter, and (a′) the corresponding SAED with the line profile. (b) A BFI of particles of 3–6 nm in mean diameter, and (*b′*) the corresponding SAED with the line profile.

In addition, in order to study the thermal stability in the alloy particles, some of the samples were then subjected to *in situ* annealing experiments. The television camera and video tape recorder (VTR) system were used for *in situ* observations. The time resolution of the VTR system, i.e., the time for one frame, was $\frac{1}{30}$ s. The micrographs were reproduced from the images recorded with the VTR system.

The microscope used was a Hitachi HF-2000 TEM equipped with a field emission gun, operating at an accelerating voltage of 200 kV. The base pressure in the specimen chamber was below 5×10^{-7} Pa, and is low enough to keep oxidation in the specimens negligibly slow. On the other hand, it was confirmed by EDS measurement that the amount of carbon and oxygen impurity in the Au-Sn alloy particles is negligibly small.

III. RESULTS AND DISCUSSION

A. Size dependence of phase stability in Au-Sn alloy particles at room temperature

Examples of size-controlled Au~35 at. % Sn alloy particles are shown in Fig. 1. Figures 1(a) and 1(a′) show a bright-field image (BFI) of particles with diameters of approximately 7–20 nm and the corresponding selected-area electron-diffraction pattern (SAED), respectively. The line profiles of the corresponding SAED's are indicated at the bottom of Figs. 1(a′) and 1(b′). In particles of larger than 10 nm in diameter, interfaces can be recognized in the interior of individual particles [as indicated with arrows in Fig. 1(a)]. As illustrated in the SAED and the corresponding line profile [Fig. 1(a′)], the Debye-Scherrer rings can be consistently indexed as those of AuSn (which has the $B8_1$ structure of the space-group $P6_3/mmc$ with lattice constants of $a_0=0.43_2$ nm and $c_0=0.55_2$ nm,) superimposed on those of Au_5Sn (which has the hexagonal structure with lattice constants of $a_0=0.50_9$ nm and $c_0=1.43_3$ nm).[11] This observation indicates that two phases were produced; one is AuSn and the other is Au_5Sn. This result is consistent with that expected from the phase diagram for the bulk material.

Figures 1(b) and 1(b′) show a BFI of particles with diameters of approximately 3–6 nm and the corresponding SAED with the line profile, respectively. In particles, no interfaces were observed in the interior of individual particles. In the SAED and the corresponding line profile [Fig. 1(b′)], two kinds of diffuse rings are recognized. The value of the scattering vector $[K=(4\pi\sin\theta)/\lambda]$ for the first diffuse ring (indicated by D_1) is approximately 22.5 nm^{-1}. Similarly, the value of the scattering vector for the second diffuse ring (indicated by D_2) is approximately 28.0 nm^{-1}. This fact indicates that a mixture of two kinds of amorphouslike alloy phases is formed and equilibrium phases in the corresponding bulk material are not produced in Au~35 at. % Sn alloy particles below 6 nm in mean diameter.

An atomic scale observation and chemical composition measurement of Au-Sn alloy particles on the same film shown in Fig. 1 have been carried out by a combination of high-resolution electron microscopy (HREM) and EDS. An example of HREM images of an approximately 20-nm-sized particle is shown in Fig. 2(a). The particle consists of two grains; grains I and II. In grain I, the 0.31-nm nm-spaced fringes are the (101) lattice fringes of AuSn. These fringes make an angle of 68° to each other, showing the incident beam direction is along the [010] direction of AuSn. In grain II, the 0.22-nm and 0.24-nm-spaced fringes are the (113) and (006) lattice fringes of Au_5Sn, respectively. These fringes make an angle of 62° to each other, showing that the incident beam direction is along the $[-110]$ direction of Au_5Sn. EDS spectra were measured in regions A and B encircled in each grain. Tin concentrations measured in regions A and B encircled were 52 and 16 at. % Sn, respectively, as shown in Fig. 2(a) and 2(b). This fact suggests that grains I and II are AuSn and Au_5Sn, respectively.

An example of HREM images of an approximately 6-nm-sized particle is shown in Fig. 2(b). The particle exhibits a contrast similar to the salt and pepper contrast reminiscent of amorphous materials. This result is consistent with the result shown in Fig. 1(b′) where diffuse rings are recognized in the SAED. An EDS spectrum measured in the encircled part of region C indicates that the tin concentration in the particle is 38 at. % Sn, as shown in Fig. 2(c). This observation indicates

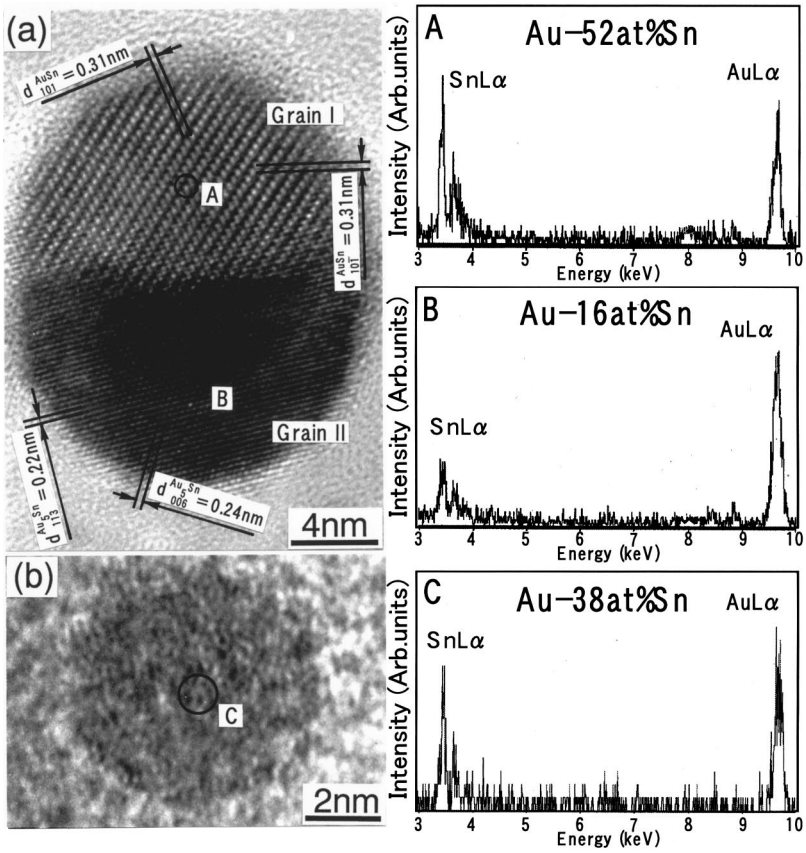

FIG. 2. (a) An example of HREM images of an approximately 20-nm-sized Au-Sn alloy particle, (b) An example of HREM images of an approximately 6-nm-sized Au-Sn alloy particle. The EDS spectra measured from regions A and B encircled. EDS spectra measured in the encircled regions of A, B, and C are shown in Figs. 2(a), 2(b), and 2(c).

that an amorphouslike phase is produced in 6-nm-sized alloy particles with the composition of 38 at. % Sn.

Figure 3 shows the changes in nanostructures of alloy particles of which the composition falls in the two-phase region as functions of both size and concentration. In this figure, marks of circle, square, and triangle indicate amorphouslike phase, Au_5Sn and AuSn, respectively. Two-phase alloy particles which consist of Au_5Sn and AuSn are shown as heavy lines connecting two marks (i.e., marks of square and triangle). In alloy particles with a diameter above 12 nm, two crystalline phases (i.e., Au_5Sn and AuSn) appear and a maximum value of the deviation from each stoichiometric composition of Au_5Sn and AuSn is about 9 at. % Sn. In approximately 10-nm-sized alloy particles, those two crystalline phases are recognized and the deviation from the stoichiometric composition of only Au_5Sn becomes remarkably high by approximately 12 at. % Sn. With decreasing particle size below 8 nm in diameter, the salt and pepper contrast characteristic of amorphouslike phases appear. It was revealed from the present experiment that in case the diameter of alloy particles is smaller than approximately 8 nm, it is difficult to form the two different phases (i.e., Au_5Sn and AuSn) in the interior of individual particles and consequently amorphouslike phases are formed, even if the composition of alloy particles falls in the two-phase region in the phase diagram for the bulk material.

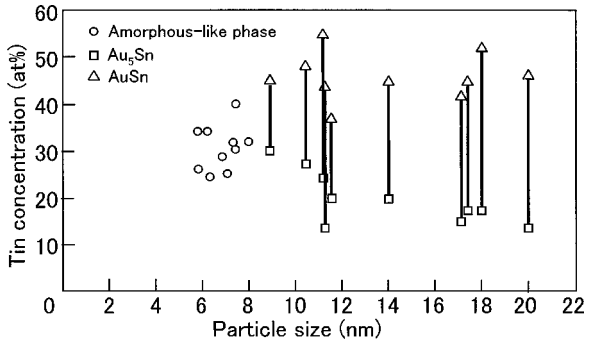

FIG. 3. Changes in nanostructures of alloy particles of which the composition falls in the two-phase region as functions of both size and concentration.

B. Temperature dependence of phase stability in approximately 5-nm-sized Au-Sn alloy particles

In order to see atomistic structures of Au-Sn alloy particles with annealing, *in situ* HREM observation has been carried out. Figure 4 is a typical sequence of the annealing process in an approximately 5-nm-sized Au 36 at. % Sn alloy particle. Figures 4(a)–4(d) show the same particle under annealing conditions. Figure 4(a) shows the particle kept at 293 K. In the particle, there appears a salt and pepper contrast reminiscent of an amorphouslike structure. Figure 4(b) shows the same particle kept at 473 K below bulk melting temperature (i.e., 551 K). The salt and pepper contrast in the particle becomes poor. The particle is neither a crystalline phase nor liquid phase at this temperature. Figure 4(c) shows the same particle kept at 773 K above bulk melting temperature. The salt and pepper contrast disappears completely and

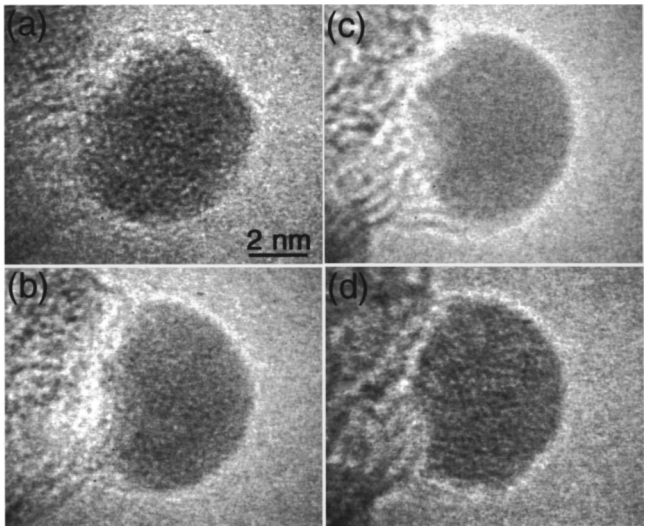

FIG. 4. A typical sequence of annealing process in an approximately 5-nm-sized Au 36 at. % Sn alloy particle.

changes into a monotonous contrast characteristic of a liquid phase. Figure 4(d) shows the same particle after cooling down to 293 K. Such a salt and pepper contrast as observed in Fig. 4(a) is recognized again. From these results, it was revealed that in a 5-nm-sized Au 36 at. % Sn alloy particle an amorphouslike phase directly changes into a liquid phase with increasing temperature from 293 to 773 K and then the reversible transformation occurs with decreasing temperature from 773 to 293 K. It was confirmed that any crystallizations does not take place with increasing or decreasing temperature.

C. Stability of amorphouslike phase in nm-sized alloy particles

In our preliminary experiments, it was confirmed that when the diameters of alloy particles become less than a few nm, the amorphouslike nanostructure (including an ultrafine grain structure) appears in the Au-In, Au-Al, and Au-Sb system which has negative heat of mixing, even if the composition of the alloy particles falls in the two-phase region in the bulk phase diagram. These results suggest that thermodynamics of alloy formation plays an important role in the formation of the amorphouslike phase in alloy particles.

The observed phase stability in nm-sized alloy particles is discussed from the viewpoint of melting temperature depression in nm-sized particles. The free energy in nm-sized solid or liquid particles will become higher than that in the corresponding bulk materials, since the fraction of atoms associated with the surface (i.e., the surface energy) increases with decreasing particle size. The increase of the free energy in solid particles in which the lattice softening[12–14] and morphological fluctuations[15,16] will be enhanced with decreasing particle size should become relatively more than that in particles in the liquid state in which the constituent atoms actively move even in the bulk materials. Consequently, it is considered that free energy as a function of temperature in nm-sized alloy particles may be changed, as shown by the schematic illustration of free-energy temperature-composition diagram in the eutectic system in Fig. 5(a). The increase (uniformly upper sift) of the free energy in nm-sized solid particles leads to the melting temperature depression. In addition, an amount of the melting temperature depression is dependent on the temperature gradient of the free energy. The temperature gradient of the free energies decreases with decreasing temperature, and then becomes significantly small at the bottom of the deep valley of the eutectic system. In the present experiments, it is shown that an amorphouslike phase is produced in nm-sized particles with the composition from about 25 to 40 at. % Sn. This composition is very close to the bottom of the deep valley of the liquids in the middle of the Au_5Sn and AuSn two-phase region in the bulk phase diagram. In fact, the eutectic point appears at a temperature as low as 551 K at 29 at. % Sn (cf. the melting point of gold of 1337 K). The increase of the free energy in nm-sized solid alloy particles which has a small temperature gradient at a reduced temperature may lead to the large depression of the eutectic temperature [eutectic temperature depression ΔT_E is larger than melting temperature depression ΔT_M, as shown in Fig. 5(a)]. It is not so difficult to show that the melting point depression of nm-sized alloy particles in the composition range near the deep eutectic point in the bulk phase diagram can be greatly enhanced as compared to that of the constituent pure substances with relatively higher melting points. The value of the melting temperature in approximately 8-nm-sized gold particles is about 1200 K,[17] and is depressed by approximately 140 K as compared to that in bulk gold (i.e., 1337 K). The value of the temperature gradient of the free energy in the solid phase estimated at the melting temperature in bulk gold is $\sim 3.8\times 10^{-2}$ kJ/mol K.[18] On the assumption that the temperature gradient of the free energy at the melting temperature in the solid phase is close to that in the liquid phase, the increase of the free energy in the solid phase, approximately 5 kJ/mol, is required to depress the melting temperature by approximately 140 K. In order to estimate approximately the temperature gradient of the free energy at the eutectic temperature (i.e., 551 K) in Au 29 at. % Sn alloy, the temperature gradient of the free energy at the same temperature in bulk pure gold was adopted because it is expected that the temperature gradient of the free energy in pure gold is close to that in Au 29 at. % Sn alloy in spite of the difference in the absolute values of the free energy. The temperature gradient of the free energy at 551 K in bulk pure gold is $\sim 1.6\times 10^{-2}$ kJ/mol K.[18] Using this value of the temperature gradient of the free energy, the value of the increase of the free energy in nm-sized solid alloy particles, approximately 5 kJ/mol will bring about the melting temperature depression of more than 300 K. This estimation is consistent with the results by Allen and Jesser[19] that the melting temperature depression of the nanoparticles in the composition range near the deep eutectic point can be greatly enhanced as compared to that of the constituent pure substances with relatively higher melting points in the calculation of the size dependence of the phase diagram for the Sn-Bi alloy nanoparticles. Figure 5(b) shows the schematic illustration of a model for amorphouslike phase formation by melting (eutectic) temperature depression in nm-sized par-

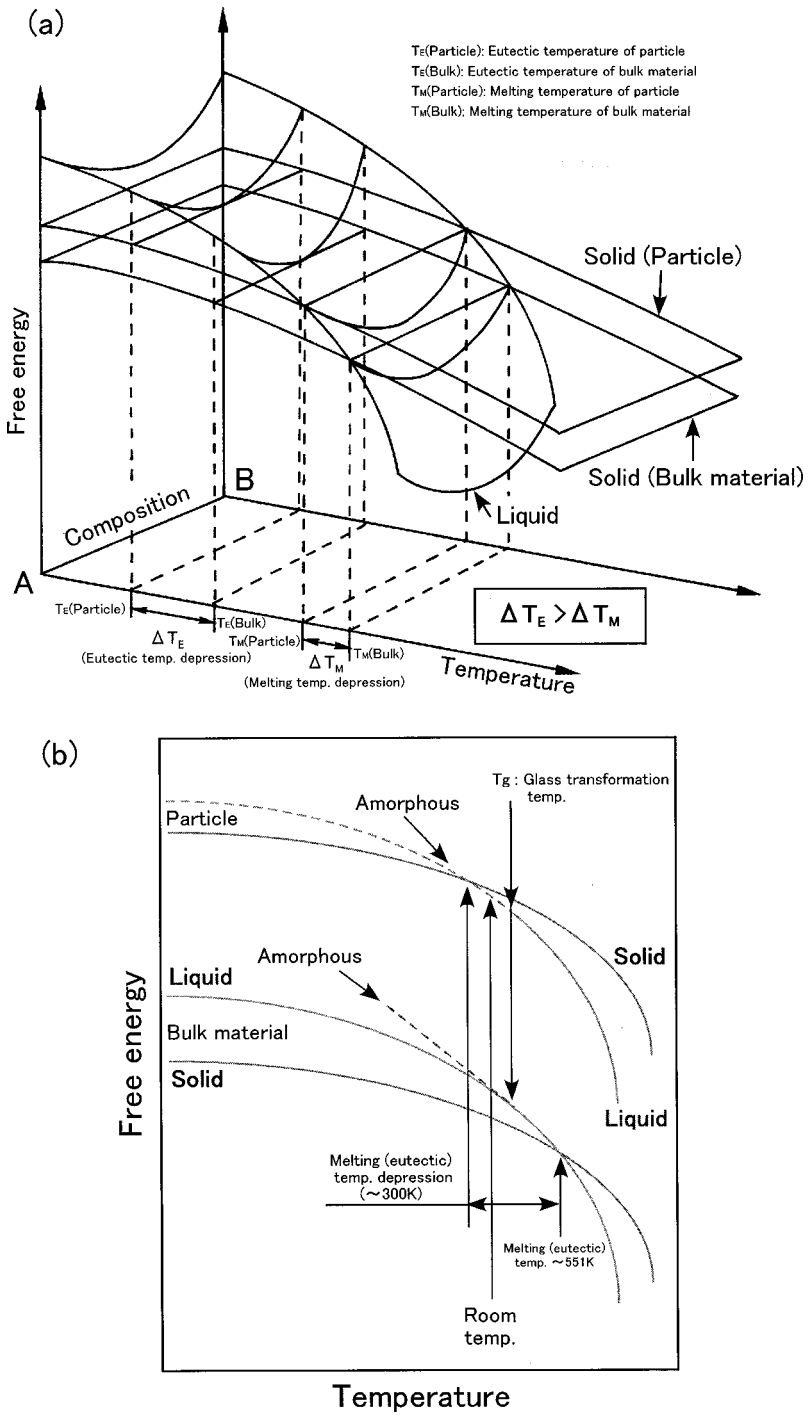

FIG. 5. Schematic illustrations of difference in the free energy between bulk materials and the corresponding nm-sized particles. (a) The schematic illustration of free-energy temperature-composition diagram in the eutectic system. (b) The schematic illustration of a thermodynamic model for amorphouslike phase formation by melting (eutectic) temperature depression in nm-sized particles.

ticles. In this case, the melting point of such nm-sized alloy particles would be below room temperature (that is, below glass transformation temperature), since the eutectic point is 551 K for bulk. Then there will be a possibility that room temperature is too low to keep the equilibrium liquid phase in the liquid state and therefore the liquid phase freezes into an amorphouslike solid phase (i.e., the ideal glass) at room temperature where the present observations were carried out. This may be one possible explanation for the formation of the amorphouslike phase. It was revealed in the previous session that the amorphouslike phase goes to melt without preceding crystallization on heating. This fact shows that the phase is not a nonequilibrium phase. In this context, the phase is different from such nonequilibrium amorphous alloy as produced by liquid quenching, mechanical grinding, or mechanical alloying.

IV. CONCLUSION

The effect of particle size on the phase stability in nm-sized Au-Sn alloy particles has been studied by TEM. When the composition of alloy particles falls in the two-phase region in the phase diagram for the bulk material, two phases expected from the phase diagram were produced in particles

of larger than 10 nm in diameter, whereas an amorphouslike phase was produced below 6-nm-sized alloy particles. The amorphouslike phase directly changes into a liquid phase with increasing temperature and then the reversible transformation occurs with decreasing temperature. The changes in the free energy in nm-sized particles bringing about melting temperature depression may play an important role in the stability of amorphouslike phases.

ACKNOWLEDGMENT

This work was supported by the ''Research for the Future'' Program, JSPS #96P00305.

*Corresponding author. Fax: +81-78-803-6129. Email address: yasuda@mech.kobe-u.ac.jp

[1] M. Takagi, J. Phys. Soc. Jpn. **9**, 359 (1951).
[2] J. R. Sambles, Proc. R. Soc. London, Ser. A **324**, 339 (1971).
[3] G. L. Allen, R. A. Bayles, W. W. Gile, and W. A. Jesser, Thin Solid Films **144**, 297 (1986).
[4] T. Castro, R. Reinfenberger, E. Choi, and R. P. Andres, Phys. Rev. B **42**, 8548 (1990).
[5] H. Yasuda and H. Mori, Z. Phys. D: At., Mol. Clusters **37**, 181 (1996).
[6] L. S. Palatnik and B. T. Boiko, Phys. Met. Metallogr. **11**, 119 (1961).
[7] G. L. Allen and W. A. Jesser, J. Cryst. Growth **70**, 546 (1984).
[8] H. Okamoto and T. B. Massalski, in *Binary Alloy Phase Diagrams*, edited by T. B. Massalski, J. L. Murray, L. H. Bennet, H. Baker, L. Kacprzak, W. W. Scott, Jr., B. P. Burton, T. Weintraub, J. Bhansali, C. E. Sirofchuck, and J. S. Sims (American Society for Metals, Metals Park, OH, 1986).
[9] H. Yasuda and K. Furuya, Eur. Phys. J. D **10**, 279 (2000).
[10] L. A. Gilifalco, *Atomic Migration in Crystals* (Blaisdell, Waltham, MA, 1964).
[11] P. Villars and L. D. Calvert, *Pearson's Handbook of Crystallographic Data for Intermetallic Phases* (American Society for Metals, Metals Park, OH, 1985).
[12] J. Harada and K. Ohshima, Surf. Sci. **106**, 51 (1981).
[13] K. Ohshima, T. Yoshiyama, and J. Harada, J. Phys. C **18**, 3073 (1985).
[14] U. Buck and R. Krohne, Phys. Rev. Lett. **73**, 947 (1994).
[15] L. D. Marks and P. M. Ajayan, Ultramicroscopy **20**, 77 (1986).
[16] P. M. Ajayan and L. D. Marks, Phys. Rev. Lett. **60**, 585 (1988).
[17] D. A. Buffet and J. P. Boel, Phys. Rev. A **13**, 2289 (1976).
[18] R. Hultgren, P. D. Desai, D. T. Hawkins, M. Gleiser, and K. K. Kelley, *Selected Values of the Thermodynamic Properties of Binary Alloys* (American Society for Metals, Metals Park, OH, 1973).
[19] W. A. Jesser, G. J. Shiflet, G. L. Allen, and J. L. Crawford, Mater. Res. Innovations **2**, 211 (1999).